

A near zero velocity dispersion stellar component in the Canes Venatici dwarf spheroidal galaxy¹

R. Ibata², S. Chapman³, M. Irwin⁴, G. Lewis⁵, N. Martin²

² *Observatoire de Strasbourg, 11, rue de l'Université, F-67000, Strasbourg, France*

³ *California Institute of Technology, Pasadena, CA 91125, U.S.A*

⁴ *Institute of Astronomy, Madingley Road, Cambridge, CB3 0HA, U.K.*

⁵ *Institute of Astronomy, School of Physics, A29, University of Sydney, NSW 2006, Australia*

13 August 2018

ABSTRACT

We present a spectroscopic survey of the newly-discovered Canes Venatici dwarf galaxy using the Keck/DEIMOS spectrograph. Two stellar populations of distinct kinematics are found to be present in this galaxy: an extended, metal-poor component, of half-light radius $7.8_{-2.1}^{+2.4}$, which has a velocity dispersion of $13.9_{-2.5}^{+3.2}$ km s⁻¹, and a more concentrated (half-light radius $3.6_{-0.8}^{+1.1}$) metal-rich component of extremely low velocity dispersion. At 99% confidence, the upper limit to the central velocity dispersion of the metal-rich population is 1.9 km s⁻¹. This is the lowest velocity dispersion ever measured in a galaxy. We perform a Jeans analysis on the two components, and find that the dynamics of the structures can only be consistent if we adopt extreme (and unlikely) values for the scale length and velocity dispersion of the metal-poor population. With a larger radial velocity sample and improved measurements of the density profile of the two populations, we anticipate that it will be possible to place strong constraints on the central distribution of the dark matter in this galaxy.

1 INTRODUCTION

Kinematical analyses of the dwarf satellite galaxies show them to be the astrophysical structures with the highest measured fraction of dark matter, with some claims of the fraction of total to luminous matter exceeding $M/L \sim 500$ (Kleyna et al. 2005). Until recently, only 11 such dwarf galaxies were known to orbit the Milky Way, however analysis of the Sloan Digital Sky Survey (SDSS) has revealed the presence of several lower luminosity dwarf galaxies that had remained undetected due to their extremely low surface brightness. Among the newly-discovered dwarf spheroidal galaxies (dSph) uncovered by the SDSS is Canis Venatici (CVn), a small structure located at a distance of approximately 220 kpc (Zucker et al. 2006). The CVn dSph has an absolute magnitude of $M_V = -7.9 \pm 0.5$, similar to the Draco dSph ($M_V = -8.8$, Mateo 1998), a Milky Way satellite galaxy 71 kpc distant (Odenkirchen et al. 2001) that provides us with one of the strongest cases for containing an extremely large fraction of dark matter. CVn is somewhat more extended than Draco however, possessing a half-light radius of 550 pc (or $8'.5$, Zucker et al. 2006), compared to 200 pc ($9'.7$, Wilkinson et al. 2002) for Draco. Although

Draco is one of the most convincing examples that dwarf galaxies possess huge mass-to-light ratios, the tidal effects of the Milky Way on this galaxy are a significant concern for analyses of its dark matter content, and the dark matter properties that have been deduced from this galaxy are contingent on the system not being significantly tidally perturbed. For this reason the CVn dwarf is an interesting candidate for a follow-up study to understand the dark matter. It is similar to Draco, but more distant, and can be expected therefore to suffer less from the Galactic tides, a reasonable assertion supported by the larger half mass radius. Here we present a first spectroscopic study aimed to reveal the dark matter properties of this intriguing galaxy.

2 OBSERVATIONS

Target stars for observation with DEIMOS were drawn from the SDSS using simple colour-magnitude criteria designed to select from the upper red giant branch and extending down to the horizontal branch at $i \sim 22$, as displayed in Fig. 1. The DEIMOS instrument at the Keck II 10m telescope is a spectrograph capable of observing up to several hundred targets simultaneously over a field of $16' \times 5'$. On the nights of May 27 and May 28 2006 we employed this instrument to observe two fields in the CVn dSph, with exposures of 3×20 min in each field. The spectrograph was used with the highest resolution 1200 l/mm grating, giving access to the spectral region 650–900 nm, and with slits of width $0''.7$, resulting in 0.1 nm resolution spectra. The spectra were pro-

¹ The data presented herein were obtained at the W.M. Keck Observatory, which is operated as a scientific partnership among the California Institute of Technology, the University of California and the National Aeronautics and Space Administration. The Observatory was made possible by the generous financial support of the W.M. Keck Foundation.

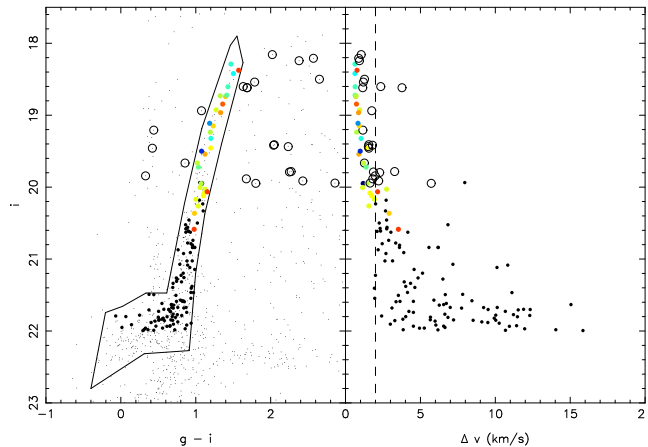


Figure 1. The colour-magnitude distribution (CMD) of SDSS stars within $10'$ of the galaxy centre is shown on the left panel. Filled circles mark the locations of the spectroscopically-observed stars that lie in the selection box, while open circles are low-priority “filler” targets. The radial velocity uncertainties are displayed in the right hand panel. The colour of the filled circles indicate the metallicity of the star; the same coding is used as in Fig. 3. Only those stars with $S/N > 15$ are coloured.

cessed using the standard pipeline developed by the DEEP2 collaboration (Davis et al. 2003), with wavelength calibration performed by comparison to a Th-Ar-Ne-Xe arc-lamp exposure taken immediately after the target observations in order to ensure the best possible velocity accuracy. The signal to noise per pixel for the brightest CVn stars was $S/N > 50$, degrading to $S/N \sim 3$ for targets at $i = 22$.

The velocities of the stars were measured by cross-correlating the observed spectra with a synthetic spectrum containing the three prominent absorption lines of the Ca II “triplet”, and the corresponding radial velocity uncertainties were estimated from the rms scatter of measurements to the three lines fit separately. As shown on the right-hand panel of Fig. 1, the radial velocity uncertainties for the brightest stars are excellent, being below 2 km s^{-1} to $i = 20$, and rise as expected in fainter targets as the signal to noise decreases. We also measure the $[\text{Fe}/\text{H}]$ metallicities of the stars with the same fitting procedure, via the equivalent width of the Ca II triplet lines (Rutledge, Hesser & Stetson 1997). The metallicities are placed on the Carretta & Gratton (1997) scale using the relation $[\text{Fe}/\text{H}] = -2.66 + 0.42[\Sigma Ca - 0.64(V_{\text{HB}} - V)]$, with $\Sigma Ca = 0.5EW_{\lambda 8498} + 1.0EW_{\lambda 8542} + 0.6EW_{\lambda 8662}$, V_{HB} being a surface gravity correction relative to the V-band magnitude of the horizontal branch, and V the V-band magnitude of the target CVn stars. For this, the V-band flux is calculated from SDSS colours using transformations derived by our group (Ibata et al., in prep.). We adopt $V_{\text{HB}} = (m - M) - 0.7 = 22.5$; although this is an approximate estimate, the derived $[\text{Fe}/\text{H}]$ is not very sensitive to this quantity, and the relative metallicity measurements are of course unaffected. A further concern is that V_{HB} is a function of age and metallicity, though choosing a single value for the mean likely incurs an additional uncertainty of less than 0.1 dex in $[\text{Fe}/\text{H}]$ (Cole et al. 2004). Previous experience has shown that below $S/N > 15$ (corresponding to $[Fe/H] \sim 0.2$) metallicity measurements become unreli-

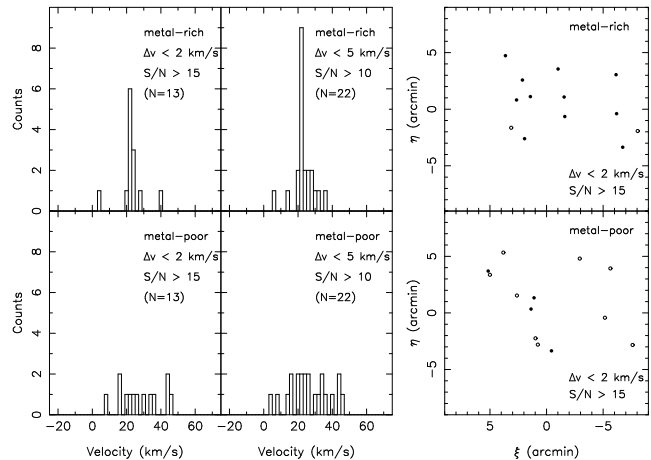


Figure 2. The velocity distribution for Samples A and B are shown on the left and middle panels, respectively, while the upper and bottom panels display, respectively, the metal-rich and metal-poor halves of each sample. The upper left-hand panel shows the presence of a velocity spike at 22.6 km s^{-1} , with rms dispersion of 1.7 km s^{-1} . The sky positions in Sample A are shown on the right-hand panels, with the full circles denoting stars within 3σ of the velocity peak.

able. Inspection of the right-hand panel of Fig. 1 shows that this signal to noise limit corresponds to a velocity uncertainty of $\Delta v \sim 2 \text{ km s}^{-1}$. We therefore adopt $S/N > 15$ and $\Delta v < 2 \text{ km s}^{-1}$ to select our more reliable measurements, which we label “Sample A”, and which contains 26 stars. In order to test the statistical limitations of this small sample, we consider a less restricted selection “Sample B”, with $S/N > 10$ and $\Delta v < 5 \text{ km s}^{-1}$, which contains 44 stars.

3 SPECTROSCOPIC RESULTS

A first inspection of the data showed a striking dichotomy between the metal-rich and metal-poor stars. Dividing Sample A into a metal-rich half and a metal-poor half, reveals a narrow peak in the metal-rich sub-sample that is not present in the metal-poor sub-sample, as shown in the left-hand panels of Fig. 2. The peak appears to contain 11 stars, and is centred at 22.6 km s^{-1} with an rms dispersion of 1.7 km s^{-1} (i.e. before removing instrumental effects). A further 2 stars are present in this selection, although displaced by more than 10σ from this narrow peak. As we relax the maximum velocity uncertainty limit to $\Delta v < 5 \text{ km s}^{-1}$ (Sample B), the peak is reinforced, as we show in the middle panels of Fig. 1, though it becomes smeared, consistent with the increased instrumental uncertainty. The F-test indicates that the probability that these two samples have the same variance is very low, 1.8×10^{-3} . This first cursory inspection of our CVn dSph sample therefore indicates that this galaxy possesses a metal-rich component with very small velocity dispersion of 1.7 km s^{-1} , together with a kinematically hotter component of lower metallicity. The stars within the two components are broadly distributed over the observed area, as demonstrated in the right-hand panels of Fig. 1.

Given this exceedingly low central velocity dispersion it is relevant to ask whether these stars are remnants of a disrupted star cluster. The right-hand panel of Fig. 3 shows the

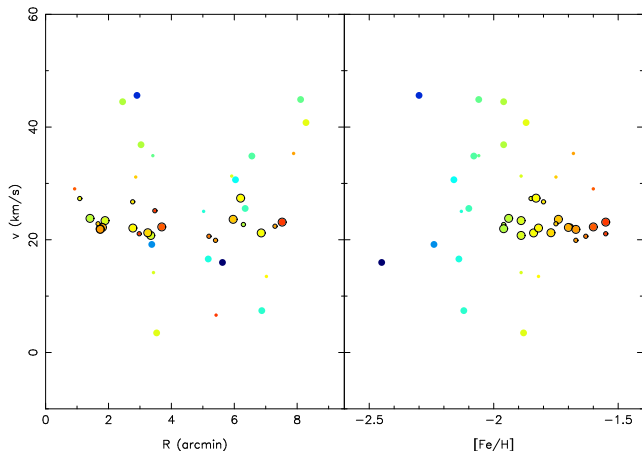


Figure 3. The velocity-radius and velocity-metallicity relations for Sample A (large dots), and Sample B (small dots). The clear grouping of metal-rich stars with $[\text{Fe}/\text{H}] > -2.0$ and with $17.5 < v < 27.7 \text{ km s}^{-1}$ are circled in this panel. The radial location of these stars is indicated in the left-hand panel (with the same colour code for metallicity). The CVn dSph evidently contains stars with a wide range of metallicities, and includes stars at the lowest end of the abundance distribution of this class of galaxies.

metallicity-velocity relation of Samples A and B. It is clear from this diagram that the stars that partake in the narrow velocity peak shown previously in Fig. 2 cover a broad range of metallicity from $[\text{Fe}/\text{H}] = -2.0$ to -1.5 . This shows conclusively that CVn became chemically enriched progressively over time, a clear sign of a galaxy that possesses (or once possessed) sufficient mass to retain and enrich gas. In contrast, star clusters have simple coeval populations of single metallicity, with the notable exception of ω Cen, which is thought to have been the core of a now disrupted dwarf galaxy (see e.g., Bekki & Norris 2006).

Fig. 3 shows that it is natural to divide CVn into a dynamically-cold, metal-rich component (circled points), and a dynamically hot, metal-poor component (the remaining non-circled points). Such behaviour has previously been discovered in the Sculptor dSph (Tolstoy et al. 2004). The boundary between the subsets was chosen at $[\text{Fe}/\text{H}] > -2.0$ and $17.5 < v < 27.7 \text{ km s}^{-1}$ (i.e. 3σ from the peak in Fig. 2); in the discussion below, we refer to the stars within this selection region as the “metal-rich component” and those outside as the “metal-poor component”. We use a maximum-likelihood technique (Fisher 1922) to correct for the individual radial velocity uncertainty estimates and thereby measure the intrinsic velocity dispersions of these components. The 13 Sample A stars belonging to the metal-rich selection display a velocity dispersion of 0.5 km s^{-1} with a 99% upper limit of 1.9 km s^{-1} (the corresponding likelihood contours are displayed in red on the right-hand panel in Fig. 4). In contrast, the 13 Sample A stars in the metal-poor selection are found to have $\sigma_v = 13.9^{+3.2}_{-2.5} \text{ km s}^{-1}$ (likelihood contours displayed dark blue in Fig. 4). With the looser selection criteria of Sample B, we measure $\sigma_v = 0.5 \text{ km s}^{-1}$, with an upper limit of 1.8 km s^{-1} (99% confidence) for the metal-rich selection, and $\sigma_v = 12.5^{+2.1}_{-1.8} \text{ km s}^{-1}$, with a lower limit of 8.7 km s^{-1} (99% confidence) for the metal-poor selection. Essentially identical results are therefore obtained from the different quality cuts of Samples A and B.

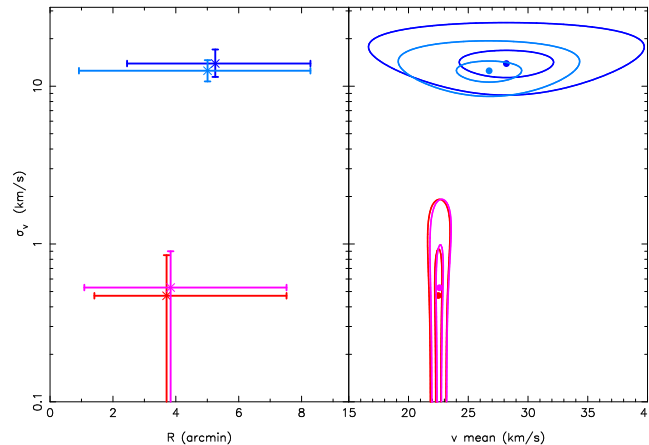


Figure 4. The likelihood contours (at 68.3% and 99%) of a Gaussian fit to the stellar sample displayed in Fig. 3 are shown in the right-hand panel, as a function of velocity dispersion and mean velocity. Dark red and dark blue correspond, respectively, to the metal-rich and metal-poor selections from Sample A, while pink and light blue show, respectively, the results from the metal-rich and metal-poor selections from Sample B. The mean radial location of the samples are shown in the left-hand panel; here the vertical bars show the 1σ velocity dispersion uncertainty, while the horizontal bars show the full radial range in each sub-sample.

4 STRUCTURE OF CVN REVISITED

We have attempted a reanalysis of the spatial structure of CVn using SDSS photometry. Given the strong chemical differences in the two kinematic components, we hoped to be able to disentangle the two populations using the colour of the red-giant branch (RGB) stars. Unfortunately, no significant differences were discovered dividing the RGB sample into blue and red sub-samples. The reason for this failure is evident from an inspection of the left-hand panel of Fig. 1, which demonstrates that there is a very small difference in RGB colour between stars of very different (spectroscopically-measured) metallicity, indicating that the metal-rich stars are substantially younger than the metal-poor stars. An alternative diagnostic that has proved to be useful in previous analyses of dSph is the comparison between the blue and red horizontal branches (HB) (Tolstoy et al. 2004). To this end we divided the CMD selection box of Fig. 1 into a blue HB (stars with $g - i < 0.2$), a red HB sample (all stars with $0.2 < g - i < 0.6$) and an RGB sample (all remaining stars in the CMD selection polygon). The corresponding contours of star density are displayed in Fig. 5. Though the blue and red HBs are very similar it is surprising to find their centres displaced from that of the RGB sample. Inspection of deeper Subaru/Suprimecam data, for which unfortunately only i-band images were available, reveal that approximately half of the sources in the SDSS HB peak are in fact due to faint galaxies which are detected as unresolved point-sources in the SDSS. However, the correction for this contamination does not make the HB peak disappear entirely. Unfortunately, the Subaru data were taken at very high airmass and do not sample the galaxy uniformly. To prove or dismiss the reality of the offset HBs (itself a very puzzling phenomenon!) will require better quality data.

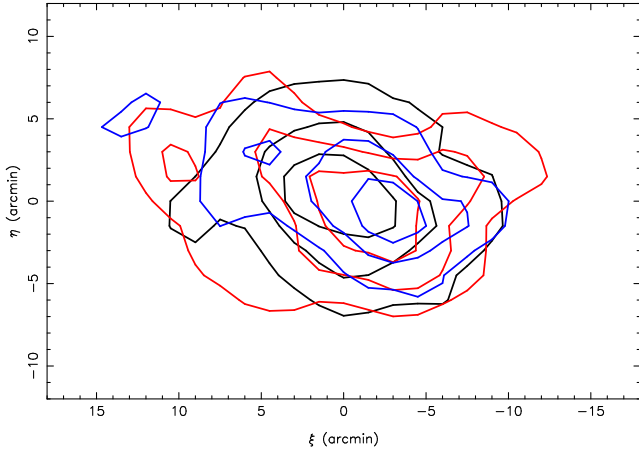


Figure 5. The SDSS stellar density contours of the RGB sample (black), the blue HB sample (blue) and the red HB sample (red).

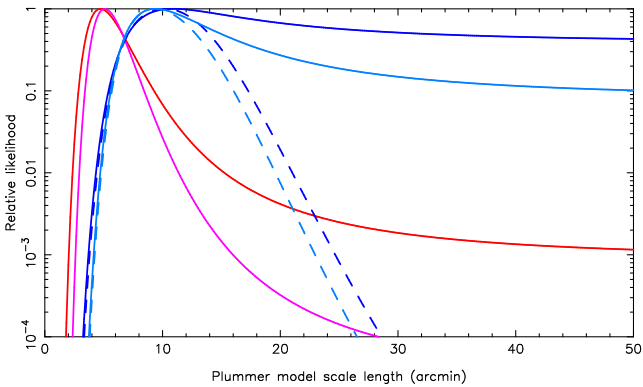


Figure 6. The relative likelihood of Plummer model fits to the metal-rich (red and pink) and metal-poor (dark blue and light blue) samples, as a function of the Plummer model scale parameter a . The same colour coding is used as in Fig. 4. Full lines use only the spectroscopically observed stars, while dashed lines complement these with SDSS photometry.

Despite the fact that the SDSS imaging data do not allow us to separate the radial profiles of the two kinematic populations, we can attempt to constrain these profiles using the DEIMOS dataset. All of the bright stars with $S/N > 10$ within the selection box of Fig. 1 were chosen by the DEIMOS slitlet configuration program with identical priorities. Assuming that the target selection program does not bias object allocation with radius, our sample can be considered to trace the two populations within the spatial “window function” of the two DEIMOS fields. We fit a Plummer model to the samples previously displayed in Fig. 4, using a maximum-likelihood method. The relative likelihood of the value of the Plummer scale length a is displayed in Fig. 6 (note that the conversion to half-mass radius is $r_h = a\sqrt{2^{2/3} - 1}$). For Sample A, the most likely value for the metal-rich component (shown in red) is $a = 4'.7$, while the metal-poor component (shown in a continuous dark blue line) is much more extended, with the most likely value of a being $10'.9$, though much larger values of a are acceptable. Of course the reason that very large values of a are acceptable is simply that the kinematic sample is confined

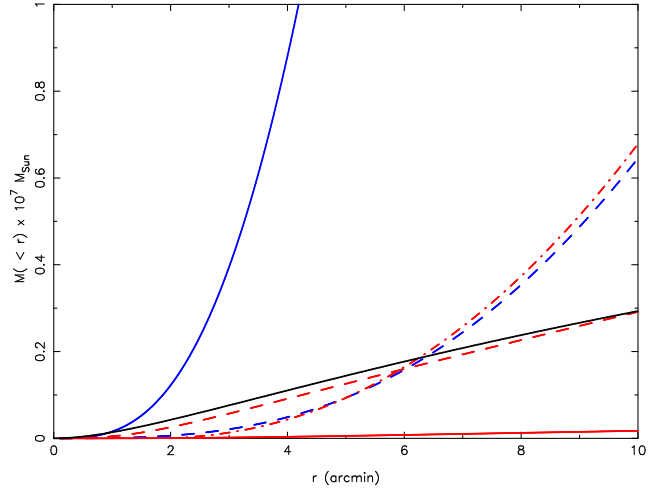


Figure 7. The enclosed mass as a function of radius. Results for the metal-poor sub-component are shown in blue. The full line shows the preferred model, which has an isothermal dispersion of $\sigma_v = 13.9 \text{ km s}^{-1}$ and Plummer scale length of $a = 10'.2$, while the dashed line is an attempt to minimise the enclosed mass and has $\sigma_v = 6.4 \text{ km s}^{-1}$ and $a = 21'$. The red lines are the mass profiles derived from the metal-rich population. The full line shows again the consequence of adopting the most likely parameters: an isothermal velocity dispersion of $\sigma_v = 0.5 \text{ km s}^{-1}$ and a Plummer scale parameter of $a = 4'.7$, while the dashed line shows an extreme model having $\sigma_v = 1.9 \text{ km s}^{-1}$ and $a = 2'.4$. The dot-dashed line is an attempt to reconcile the mass profile of the metal-rich sub-system with the metal-poor sub-system: it possesses the preferred Plummer scale length of $a = 4'.7$, but has linearly increasing velocity dispersion profile with a central value of $\sigma_v = 1.5 \text{ km s}^{-1}$, increasing to $\sigma_v = 3.2 \text{ km s}^{-1}$ at $6'.6$. For comparison, we superimpose the mass profile of a Navarro, Frenk & White (1997) model of Virial mass $10^7 M_\odot$ and concentration $c = 20$ (black line).

to $R < 9'$. To improve the constraint on a we supplement the metal-poor star sample with RGB stars detected in the SDSS, at radii between $9'$ (i.e., twice the scale length of the metal-rich component) and $24'$ (where the profile disappears into the background). The corresponding likelihood curve is displayed in Fig. 6 with a dashed dark blue line, and possesses a maximum at $a = 10'.2$, similar to the result from the kinematic sample alone, but falls off rapidly for large a . Very similar results are derived for Sample B (see Fig. 6). We therefore find that the metal-rich population is more centrally concentrated than the metal-poor population.

5 DISCUSSION

The upper limit to the velocity dispersion of the metal-rich component in CVn is the lowest ever measured in a galaxy. As such, it presents a fascinating problem for galaxy formation. The simplest explanation may be that CVn was a normal dark-matter dominated dSph that has been severely tidally disrupted over time. The removal of the extended dark matter halo of the galaxy by tidal forces could lower the central velocity dispersion of the stellar component by lowering the mass of the system. In this interpretation, the higher dispersion in the external regions would attest to ongoing tidal disruption of the outermost stars. However, the

regular contours found by Zucker et al. (2006) are suggestive of only mild tidal forces, which argues against this scenario.

Assuming that the system is in dynamical equilibrium, we may apply the Jeans equations to deduce the mass profile of the dwarf galaxy, including the dark matter. With the further assumptions that the galaxy is spherically symmetric, that the two stellar components follow the (projected) Plummer density distributions fitted previously, and that there is no appreciable velocity anisotropy, the Jeans equations can be simplified to Eqns. 4-56 and 4-58 of Binney & Tremaine (1987). The solid blue and red lines in Fig. 7 show the computed mass profiles for the metal-poor and metal-rich components, respectively, using the most likely model parameters. For this we have taken the parameters $a = 10'.2$ and $\sigma_v = 13.9 \text{ km s}^{-1}$ (metal-poor), and $a = 4'.7$ and $\sigma_v = 0.5 \text{ km s}^{-1}$ (metal-rich), with the further assumption that the velocity dispersion are constant at all radii. The two derived mass profiles could hardly be more different, and are clearly completely inconsistent with each other. To obtain a degree of consistency between the components (dashed lines), we are obliged to force the metal-poor component to $a = 21'$, $\sigma_v = 6.4 \text{ km s}^{-1}$ (the 99% upper and lower limits for these parameters, respectively), and take the opposite limits for the metal-rich component: $a = 2'.4$, $\sigma_v = 1.9 \text{ km s}^{-1}$. The combination of these extreme parameter values is highly unlikely of course, and illustrates the extent to which the two components are apparently inconsistent. However, without a more reliable description of the components it is difficult to be categorical about the inconsistency. In particular, we have little information on the radial profile of the velocity dispersion. The effect of this uncertainty is illustrated by the dot-dashed line, where we have taken the most likely Plummer scale parameter for the metal-rich structure, $a = 4'.7$, together with a linearly-increasing velocity dispersion model that has a central value of 1.5 km s^{-1} , increasing to 3 km s^{-1} at $6'$. With these parameters the mass profile required by the metal-rich component agrees very well with the extreme configuration of the metal-poor structure (blue dashed line).

6 CONCLUSIONS

We have uncovered two stellar components in the Canes Venatici dwarf spheroidal galaxy with distinct structure and kinematics. Below a metallicity of $[\text{Fe}/\text{H}] = -2$ this galaxy has a velocity dispersion of $\sim 10 \text{ km s}^{-1}$, typical of other dSph galaxies. At metallicities richer than this limit, an intriguing additional component is detected, possessing a velocity dispersion that is barely resolved with our measurement accuracy, and has an upper limit of 1.9 km s^{-1} . The nature of the metal-rich component is unclear, though the wide metallicity spread it displays suggests that it was formed in situ from gas reprocessed from the previous generation of metal-poor stars. The possibility that the metal-rich population is younger is supported by the overlap of the red-giant branches of both populations in the CMD.

Thus the CVn dwarf presents us with a very interesting puzzle: why does this younger population possess such a small velocity dispersion? Naively, one would expect this to attest to the presence of a cored potential in the central regions of the galaxy: where the potential gradients are flat one can hide much dark mass without structures that

are significantly smaller in scale than the core radius being substantially affected. However, the Jeans analysis we have performed does not support this scenario, due to the relatively small scale length of the metal-poor population. Instead, we find that the model parameters must be forced to highly unlikely extremes to achieve a reasonable consistency between the components. We feel, however, that the paucity of well-measured stars in the kinematic sample, especially at large radius, introduces a large modelling uncertainty, and we therefore avoid stating categorically at the present time that the two populations are inconsistent.

If future studies confirm the values for the velocity dispersion and component scale lengths presented here, it will be a clear indication that one or more of the assumptions made in the Jeans analysis is invalid. The system may not be in dynamical equilibrium: despite the previous discussion, it is possible that the metal-rich population is a recent accretion that has not had time to relax. Given typical dynamical times, this seems very unlikely, though we note that in other dSph fossil substructure has been detected, and its longevity can be interpreted as consistent with the presence of a cored dark matter distribution (Kleyna et al. 2003). Alternatively, the adopted assumption of spherical symmetry may be poor. The metal-rich component may also be a disk-like component seen face-on, though this is hard to envisage if it was formed from the existing apparently non-rotating metal-poor population, given the similarity in their scale lengths. It may also turn out to be that the velocity distribution is not isotropic.

Although the present uncertainties in the model parameters do not allow us to provide strong constraints on the dark matter distribution, we anticipate that if the predictions of the two components can be made consistent with improved data, this will yield a reliable dark matter profile, from which we may confidently determine whether the dark matter conforms to the predictions of CDM theory or not.

REFERENCES

- Bekki, K., Norris, J. 2006, ApJ637, 109L
- Binney, J. & Tremaine, S. 1987, Galactic Dynamics, Princeton University Press, Princeton
- Carretta, E., Gratton, R. 1997, A&AS 121, 95
- Cole, A., Smecker-Hane, T., Tolstoy, E., Bosler, T., Gallagher, J. 2004, MNRAS 347, 367
- Davis, M., et al. 2003, Proc. SPIE, 4834, 161
- Fisher, R. A. 1922, Philos. Trans. Roy. Soc. London Ser. A, 222, 309
- Kleyna, J., Wilkinson, M. I., Gilmore, G., Evans, N. W. 2003, ApJ 588, L21 MNRAS 330, 792
- Kleyna, J., Wilkinson, M. I., Evans, N. W., Gilmore, G. 2005, ApJ 630, L141 MNRAS 330, 792
- Mateo, M. 1998, ARA&A 36, 435
- Navarro, J., Frenk, C., White, S., 1997, ApJ 490, 493
- Odenkirchen, M., et al. 2001, AJ 122, 2538
- Rutledge, G., Hesser, J., Stetson, P. 1997, PASP 109, 883
- Tolstoy, E., et al. 2004, ApJ 617, L122
- Wilkinson, M. I., Kleyna, J., Evans, N. W., Gilmore G. F., 2002, MNRAS 330, 778
- Zucker, D., et al. 2006, astro-ph/0604354